IEEE Access
Multidisciplinary | Rapid Review | Open Access Journal

Received September 24, 2019, accepted October 10, 2019, date of publication October 22, 2019, date of current version November 5, 2019.

Digital Object Identifier 10.1109/ACCESS.2019.2948951

Analysis of a Novel Dual-Rotor Induction Motor for Pulsed Power Driving System

PEILONG WANG[1,2] AND LIMING SHI[1], (Member, IEEE)
[1]Key Laboratory of Power Electronics and Electric Drive, Institute of Electrical Engineering, Chinese Academy of Sciences, Beijing 100190, China
[2]School of Electronic, Electrical and Communication Engineering, University of Chinese Academy of Sciences, Beijing 100049, China

Corresponding author: Liming Shi (limings@mail.iee.ac.cn)

This work was supported in part by the Research Foundation of the Chinese Academy of Sciences under Grant 301020804.

ABSTRACT A novel dual-rotor induction motor (DRIM) is proposed as a potential substitution of the traditional motor/generator with a flywheel (MGFW) used in the pulsed power driving system (PPDS) which is especially deployed in mobile platforms. The DRIM is based on the integration of flywheel energy storage and electromagnetic slip coupling mechanism. The DRIM utilizes its outer rotor as a flywheel to store the input mechanical energy. By the interaction between the excitation field produced by the outer rotor and the eddy current induced on the surface of the inner rotor, an electromagnetic torque is generated and simultaneously acted on the two rotors. So the stored energy in the outer rotor can be directly transferred to the inner rotor with the mechanical load through the torque. The substitution of MGFW with DRIM holds potential for simplifying the PPDS and improving its compactness. The configuration and operation mechanism of the DRIM are firstly introduced in this paper. Then transient characteristics of the DRIM are analyzed by the 2D finite element method (FEM). The influences of the excitation pole number and the excitation coil turns on the performance of the DRIM are investigated. Finally, the feasibility of the DRIM is experimentally verified by a prototype.

INDEX TERMS Dual-rotor induction motor, electromagnetic slip coupling, finite element methods, flywheel energy storage, pulsed power driving system, transient electromagnetic analysis.

I. INTRODUCTION

Pulsed power driving system (PPDS) has been adopted in various applications such as the car crash test platform and the electromagnetic launcher [1]–[5]. In these applications, a huge instantaneous mechanical driving power is required for the acceleration of an inertia load in a short time. The energy storage equipment providing a huge instantaneous power plays a significant role in the PPDS. The motor/generator with a flywheel (MGFW) has been a preferred energy storage equipment employed by the PPDS due to its high power density and long life operation cycle [2]–[5]. A traditional system solution for such PPDS has been shown in Fig. 1. The system is mainly composed of a driving motor, a bidirectional converter, and a MGFW.

The PPDS shown in Fig. 1 has two operation stages, namely the energy storage stage and the driving stage. In the energy storage stage S_1 is closed and S_2 is opened. The MGFW absorbs the energy from an electrical source through a bidirectional converter and then stores them as the rotational kinetic energy in the MGFW. In the driving stage S_1 is opened and S_2 is closed. And the previously energy stored by the MGFW is released and converted by the bidirectional converter to electrical power. And a large power driving motor supplied by the electrical power drives an inertia load to achieve the instantaneous acceleration. Power flow of the traditional PPDS in different modes has also been shown in Fig. 1.

The MGWF shown in Fig. 1 is based on an electrically excited synchronous machine. And the MGFW exchanges energy with outside in the electrical form. But the energy required by the PPDS for inertia load acceleration is in the mechanical form. Therefore, even though the MGFW can provide the transient power required by the load, the multiple conversion of the stored power by a bidirectional converter and a driving motor is inevitable. However, considering the power level of a PPDS required in practice, the cooperative control of a driving motor, a bidirectional converter, and a MGFW is complicated. And the large power requirement of a bidirectional converter, a driving motor, and a MGFW

The associate editor coordinating the review of this manuscript and approving it for publication was Fabio Massaro.

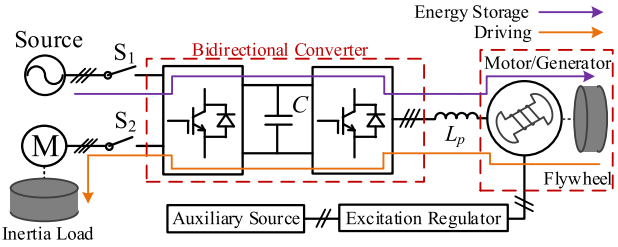

FIGURE 1. Architecture of the traditional PPDS based on a MGFW.

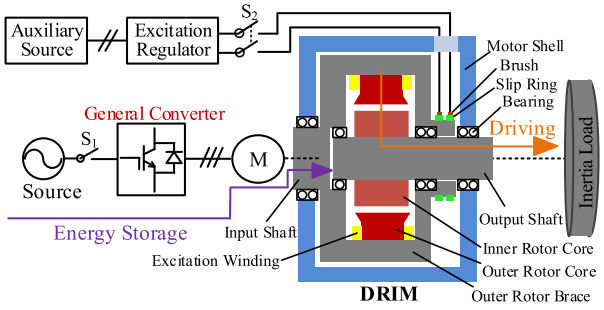

FIGURE 2. Architecture of the novel PPDS based on a DRIM.

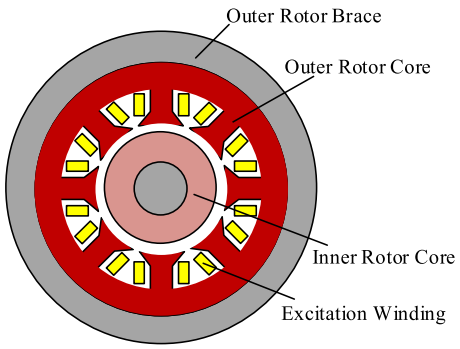

FIGURE 3. Cross section view of the DRIM (motor shell omitted).

eventually leads to a cumbersome system, which is obviously adverse to the application of a PPDS in the mobile platform with limited space and weight-carrying capacity.

In recent years, the MGFW based on different kinds of electrical machines have been proposed and investigated, for example, the BLDC machine [6], [7], the permanent magnet synchronous machine [8]–[12], the synchronous reluctance machine [13], [14], the homo-polar inductor machine [15], and the electrically excited synchronous machine [16]–[20]. However, the adoption of a MGFW based on any kind of those traditional electrical machines is inadequate to alleviate the problem of the system complexity in the PPDS.

To solve the above mentioned problem, a novel dual-rotor induction motor (DRIM) for the PPDS is proposed in this paper. The DRIM is based on the flywheel energy storage and electromagnetic slip coupling mechanism. Fig. 2 shows the architecture of the novel PPDS based on a DRIM.

Compared with the traditional PPDS based on a MGFW, the novel PPDS replaces the combination of a large power driving motor and a MGFW with that of a small power auxiliary motor and a DRIM. A large capacity bidirectional converter is also replaced with a small capacity unidirectional general converter. Furthermore, since the rotational kinetic energy storage is implemented by the outer rotor of the DRIM, the flywheel is also omitted in the novel PPDS. As a result, the substitution of a MGFW with a DRIM can be a promising method to simplify the PPDS and improve its compactness. And that is beneficial for the deployment of the PPDS in mobile platforms with the limited space and weight-carrying capacity.

In this paper, the configuration and operation principle of the DRIM are introduced firstly. Then the specification of a prototype DRIM is presented and 2D finite element method (FEM) is employed to analyze its transient electromagnetic process and driving characteristics. And influences of key structure parameters on the driving performance of the DRIM are also investigated by 2D finite element method (FEM). Finally, an experiment platform is established to experimentally confirm the feasibility of the DRIM and verify the simulation results.

II. CONFIGURATION OF DRIM

The DRIM is mainly composed of some essential structural support and two rotors, namely, an outer rotor for energy storing and an inner rotor for driving load. The fundamental structure of the proposed DRIM has been presented in Fig. 2. And its simplified cross section view is shown in Fig. 3.

In order to improve the energy storage density and driving capability of the DRIM, the inertia of the rotor for energy storage needs to be large while the inertia of the rotor for driving load needs to be small. Therefore the outer rotor is selected to store the input mechanical energy and the load is attached to the inner rotor.

The main function of the outer rotor is to store the input mechanical energy from outside by its own rotational inertia and to establish an electromagnetic coupling filed in the DRIM. The outer rotor core is made up of laminated silicon steels. The excitation winding is placed in the core slot. The excitation winding is connected to an auxiliary excitation DC voltage source through the electron brush and slip ring. The outer rotor brace and the bearings are used to provide a necessary structure supporting so that the two rotors can rotate freely from each other in the motor shell, as shown in Fig. 2. Besides, the mass of the out rotor brace can also be adjusted during structure design so that the total inertia of outer rotor meets the requirement of the energy storage. Then an additional flywheel can be omitted in the DRIM.

The function of the inner rotor is to directly drive an inertia load to accelerate. Considering the system reliability requirement and instantaneous high acceleration operation condition, a smooth solid iron core is employed by the inner rotor since it is obviously not only mechanically robust but also easily manufactured.

III. OPERATION OF DRIM IN DIFFERENT STAGES

A. ENERGY STORAGE STAGE

In the energy storage stage, the excitation winding of DRIM is disconnected from the auxiliary excitation source, so there is no electromagnetic coupling field in the DRIM. Thus, no interaction occurs between the two rotors in this stage. Outer rotor is dragged by the small power auxiliary motor and slowly accelerated to a pre-determined speed Ω_0. As a result, the input mechanical energy is stored by the out rotor of DRIM in form of kinetic energy. In this stage, the inner rotor is held standstill by an auxiliary locking device to avoid creeping. After the end of this stage, the energy stored in DRIM can be calculated as

$$E = \frac{1}{2} J_1 \Omega_0^2 \tag{1}$$

where J_1 is total rotational inertia of the outer rotor including the outer rotor core, the excitation winding, input shafts and the outer rotor brace.

B. DRIVING STAGE

In the driving stage, auxiliary locking devices of inner rotor is firstly unlocked and meantime excitation winding is fed with auxiliary DC power supply. Then the winding current is raised and electromagnetic field in DRIM is established quickly. Due to the slip speed between two rotors, alternating magnetic field is produced in inner rotor core by excitation winding current.

Owing to skin effect, distribution of magnetic field and eddy current in inner rotor core are mainly limited within the penetration depth δ as

$$\delta = \sqrt{\frac{2}{\omega \mu_0 \mu_r \sigma}} \tag{2}$$

where μ_0 is vacuum permeability; μ_r is relative permeability of inner core; σ is conductivity of inner rotor core; and ω is the electromagnetic field angular frequency relative to inner rotor and expressed as

$$\omega = 2\pi f = 2\pi \frac{\Delta\Omega}{60} p = \frac{1}{30} \Delta\Omega \pi p \tag{3}$$

where f is field frequency relative to inner rotor, and p is pole pairs of outer rotor. $\Delta\Omega$ is transient slip speed between two rotors as

$$\Delta\Omega = \Omega_1 - \Omega_2 \tag{4}$$

in which Ω_1 and Ω_2 are transient speed of outer and inner rotor, respectively. Substituting (3) and (4) into (2) gives

$$\delta = \sqrt{\frac{60}{\pi \mu_0} \frac{1}{(\Omega_1 - \Omega_2) p \sigma \mu_r}} = \sqrt{\frac{k}{(\Omega_1 - \Omega_2) p \sigma \mu_r}} \tag{5}$$

Due to the slip speed the eddy current loss p_{ec} within inner rotor is determined by

$$p_{ec} = \left(l_{ef}/\sigma\right) \int_{r1}^{r2} \int_{0}^{2\pi} |J(r, \theta)|^2 \, r dr d\theta \tag{6}$$

where l_{ef} is effective axial length of DRIM. And r_1 and r_2 are external diameter and internal diameter of inner rotor core respectively. Considering the pulse operation mode of DRIM, the relatively low efficiency caused by the eddy current loss is reasonably acceptable. Based on electromagnetic coupling mechanism theories [21]–[23] electromagnetic torque T_e is calculated by

$$T_e = \frac{p_{ec}}{\Delta\Omega} \tag{7}$$

By the effect of T_e, outer rotor will decelerate from speed of Ω_0 and inner rotor will drive load to accelerate from stationary. If the friction of shafts in DRIM is ignored, the variation of two rotor speeds in the driving stage can be expressed as

$$T_e = -J_1 \frac{d\Omega_1}{dt} = J_2 \frac{d\Omega_2}{dt} \tag{8}$$

where J_2 represents the total rotational inertia of the inner rotor and the load. Ω_1 and Ω_2 are the transient speed of outer and inner rotor, respectively. And the mechanical power released from outer rotor p_{M1} can be calculated by

$$p_{M1} = T_e \Omega_1 \tag{9}$$

whereas driving power of DRIM p_{M2} is

$$p_{M2} = T_e \Omega_2 \tag{10}$$

With the condition that friction is ignored, the system angular momentum can be assumed conservative. Therefore, after the end of driving stage, outer rotor and inner rotor reach the same final speed Ω_f, which is determined only by J_1, J_2 and Ω_0, namely

$$\Omega_f = \frac{J_1}{J_1 + J_2} \Omega_0 \tag{11}$$

On the other side, as soon as outer rotor winding is fed with DC power supply U, the establishment of the excitation winding current i can be expressed as

$$U = iR + \frac{d\psi}{dt} \tag{12}$$

where R is resistance of outer rotor winding, ψ is total flux linkage of excitation winding

$$\psi = \psi_1 - \psi_2 \tag{13}$$

where ψ_1 is flux linkage produced by excitation winding current and ψ_2 is produced by eddy current in inner rotor core. And the minus sign before ψ_2 means the demagnetizing property of eddy current for the excitation magnetic field.

The excitation power p_{1e} required by the DRIM during driving stage is calculated by

$$p_{1e} = Ui = \left(iR + \frac{d\psi}{dt}\right) i = i^2 R + i \frac{d\psi}{dt} = p_{1\Omega} + p_{1m} \tag{14}$$

The first item $p_{1\Omega}$ in right end of (14) represents the winding ohm loss power while the second item p_{1m} represents the

power absorbed by electromagnetic field from the excitation voltage source.

At the end of driving stage the outer rotor and the inner rotor rotate synchronously, so the winding flux linkage will not vary any more. At this time (14) could be rewritten as

$$P_{1e} = U\frac{U}{R} = UI = \frac{U^2}{R} \tag{15}$$

where P_{1e} and I are the maximum excitation power and excitation current required by DRIM, respectively.

It should be noted that during driving stage, magnetic field in DRIM is synchronously rotating with exciting winding due to salient structure of out rotor and its DC excitation mode. Then none motional electromotive force is produced in the excitation winding in driving stage. So exciting power p_{1e} absorbed by DRIM winding from auxiliary power source cannot be used to electromechanical energy conversion. As a result, p_{1m} is only used to establish the electromagnetic field and p_{M2} comes from p_{M1} released by the outer rotor.

In the conventional PPDS based on a GMWF, as depicted in Fig. 1, due to the unavoidable energy conversion by the bidirectional converter in the driving stage, the power ratings of the bidirectional converter is not less than the maximum driving power required for the load acceleration. However, in the following analysis, it will be demonstrated that maximum excitation power required by a DRIM is quite small when compared with its maximum driving power.

For convenience of the following investigation of ratio between the driving power and the required excitation power of DRIM, a factor λ is introduced here as

$$\lambda = \frac{P_{1e}}{P_{M2}} \tag{16}$$

where P_{M2} is the peak value of the driving power p_{M2} during the whole driving stage.

IV. FEM ANALYSIS OF DRIM

To verify the feasibility of the DRIM and analyze its operation characteristics, the FEM model of a prototype is established in this section. The prototype is used to accelerate a load from a standstill to the target speed of 1100 rpm within 450 ms. And the inertia moment of the load is 2.75 kgm^2. The specifications of the prototype studied in this section are listed in Table 1. Besides, 8 excitation coils are connected in serial and the total resistance of excitation winding is 2.63 Ω. The excitation voltage is 190 V.

Considering the end effect of eddy current induced in the inner solid rotor, the conductivity of inner rotor core material is revised by an end effect factor as in [24].

$$K = 1 - \frac{2\tau}{\pi l_{ef}} \frac{\tanh\left(\frac{\pi l_{ef}}{2\tau}\right)}{1 + \tanh\left(\frac{\pi l_{ef}}{2\tau}\right)} \tag{17}$$

where τ is the pole pitch.

The established 2D FEM mode is shown in Fig. 4(a). And Fig. 4(b) to Fig. 4(d) show the transient field distribution of DRIM at 168 ms after the start of driving stage.

TABLE 1. Specifications of the DRIM prototype.

Items	Unit	Values
Diameter of outer rotor core	mm	360
Diameter of inner rotor core	mm	200
Diameter of inner rotor shaft	mm	108
Number of outer rotor poles	-	8
Pole embrace ratio		0.67
Number of turns per coil	-	80
Air-gap length	mm	1
Effective axial length	mm	310
Energy Storage Speed of outer rotor	rpm	1500
Total inertia of outer rotor side	kgm^2	8.681
Total inertia of inner rotor side	kgm^2	3.160
Outer rotor core material	-	Laminated Steel Sheet
Inner rotor core material	-	Solid Iron
Conductivity of inner rotor core	S/m	6.67e6

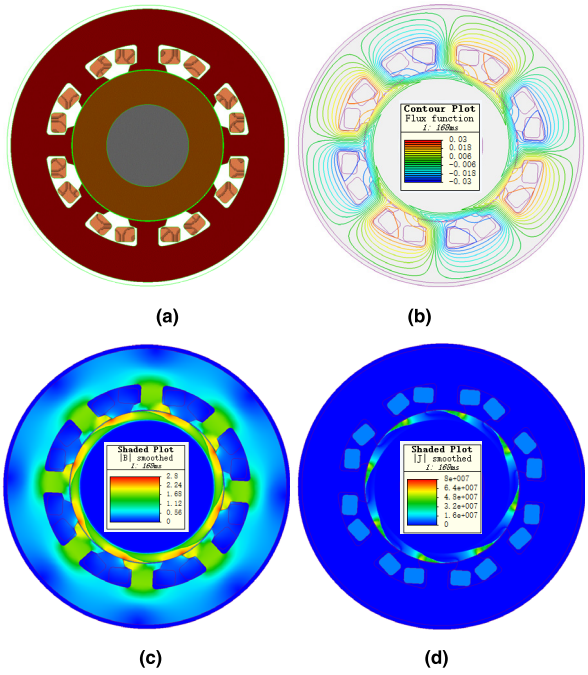

FIGURE 4. Established model and field distribution of the DRIM when time = 168ms, $\Omega_1 = 1300$ rpm, $\Omega_2 = 550$ rpm and $i = 63$A. (a) 2D FEM model. (b) Flux line. (c) Magnetic field density. (d) Eddy current.

As depicted in Fig. 4(b), the penetration depth of magnetic field in inner rotor is limited due to the slip speed between two rotors, and eddy current of inner rotor mainly distributes on its surface as shown in Fig. 4(d). So the flux distribution in inner rotor is distorted due to the effect of eddy current. It can be observed in Fig. 4(c) that outer rotor core pole shoes in clock direction side and surface of inner rotor core are highly statured, which leads to the demagnetizing property of eddy current for excitation field. The performance of DRIM in driving stage obtained by 2D FEM is shown in Fig. 5.

From Fig. 5(a), it is clear that the inner rotor begins to accelerate while the outer rotor begins to decelerate after start of driving stage, and it takes two rotors about 422 ms to reach the same speed of 1100 rpm.

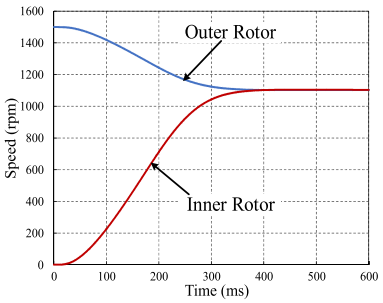

(a)

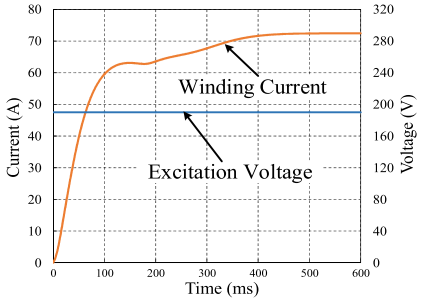

(b)

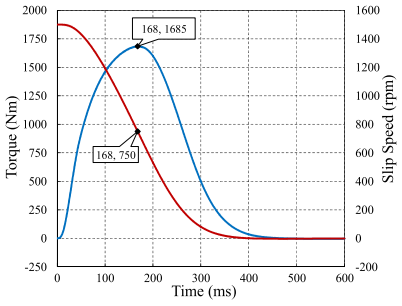

(c)

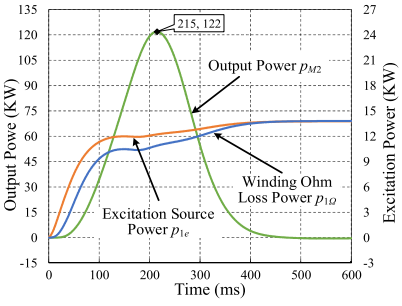

(d)

FIGURE 5. DRIM performance in driving stage when $U = 190$ V and $\Omega_0 = 1500$ rpm. (a) Rotor speed. (b) Winding voltage and current. (c) Slip speed and torque. (d) Power comparison.

During the driving stage, changing slip speed between two rotors leads to change of electromagnetic field penetration depth in inner rotor. As depicted in Fig. 5(b), the variation of current establishment is observed due to the change of magnetic circuit and the damping effect of eddy current within inner rotor, both of which are substantially influenced by penetration depth.

Fig. 5(c) shows the transient electromagnetic torque and slip speed between outer and inner rotor. It can be seen that the electromagnetic torque first increases and then decreases along with the decline of the slip speed. And the torque reaches the maximum value of 1685 Nm at the slip speed of 750 rpm.

The transient driving power and required excitation power of DRIM are compared in Fig. 5(d). The maximum driving power reaches nearly 122 KW whereas the required excitation power is only 13.73 KW. According to definition in (16), λ is less than 0.12 for DRIM under this operation condition. This means required excitation power is within 12% of maximum driving power. It endows DRIM with the ability to control the instantaneous large mechanical driving power by a relatively small excitation power. For the MGFW based on traditional electrical machines, the electrical power required in the driving stage is not less than its desired output mechanical power. That means the λ is not less than 1. So the required electrical power can be notably reduced by using the DRIM in PPDS.

Besides, it is known from results shown in Fig. 5(d) that the major part of excitation power consumes in the excitation winding resistance as ohm loss.

V. INFLUENCE OF STRUCTURE PARAMETERS ON PERFORMANCE OF DRIM IN DRIVING STAGE

According to the above analysis, main mechanical factors affecting the driving performance of a DRIM are the initial outer rotor speed and the system rotational inertia, which are previously decided by the driving requirement of the load according to (11). Meanwhile, winding resistance R and winding flux linkage ψ are main electromagnetic factors affecting the performance, which are mainly influenced by the pole number and coil turns of excitation windings.

In order to find a reasonable pole number and coil turns under the same driving requirement, the comparative analysis of DRIMs with different pole number and coil turns is conducted in this section. In the following analysis, the initial speed Ω_0 is set to 1500 rpm.

A. POLE NUMBER

Outer rotor pole geometry dimension is kept unchanged when pole number changes in this subsection. Turns of each coil and other parameters remain consistent with Table 1.

Fig. 6 shows the established FEM models of DRIM with 6 poles and 10 poles. Excitation coils in different models are connected in serial. Total winding resistance R is assumed to be directly proportional to pole pairs. So winding resistance is 1.97 Ω, 2.63 Ω, and 3.28 Ω when pole number varies from 6, 8 to 10. For the convenience of comparison, excitation voltage has been adjusted according to the difference of the winding resistance so that the maximum winding current I of different models remains same. Then the excitation voltage are 142.5 V, 190 V, and 237.5 V when the pole number varies from 6, 8 to 10. The results are shown in Fig. 7.

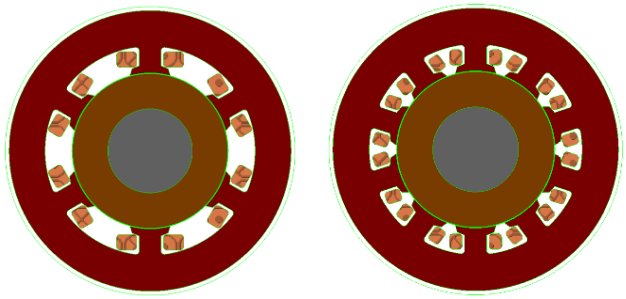

FIGURE 6. Models of DRIM with different pole pairs. (a) 6 poles. (b) 10 poles.

According to simulation results, the torque establishment is speeding up with the increase of pole number as shown in Fig. 7(b). Maximum torque is also increased and the time corresponding to maximum torque becomes short, namely 1133 Nm at 258 ms for 6 poles, 1685 Nm at 168 ms for 8 poles, and 2122 Nm at 132ms for 10 poles. As a result, it can be observed from Fig.7 (a) that time for inner rotor to reach the final speed Ω_f decreases, namely 577 ms for 6 poles, 422 ms for 8 poles, and 386 ms for 10 poles.

The improvement in driving performance can be mainly attributed to rise of total winding ampere turns along with pole number increase, as shown in Fig. 7(c). According to the obtained power comparison between maximum driving power and required maximum excitation power as shown in Fig. 7(d), it can be seen that both of them raise along with pole number increase. But the factor λ approximately remains unchanged, which means that the increase of pole number can improve the transient driving ability without a remarkable enlargement of required excitation power.

However, as shown in Fig. 7(a), the driving performance improvement by the increase of pole number is gradually indistinct in terms of the load acceleration time. Besides, it is known that a large pole number also leads to the small slot notch and slot area when the inner radium of outer rotor is unvaried. Therefore, even though the DRIM with 10 poles possesses the most powerful transient driving ability, an 8 poles design scheme is more reasonable and is selected in the following prototype design.

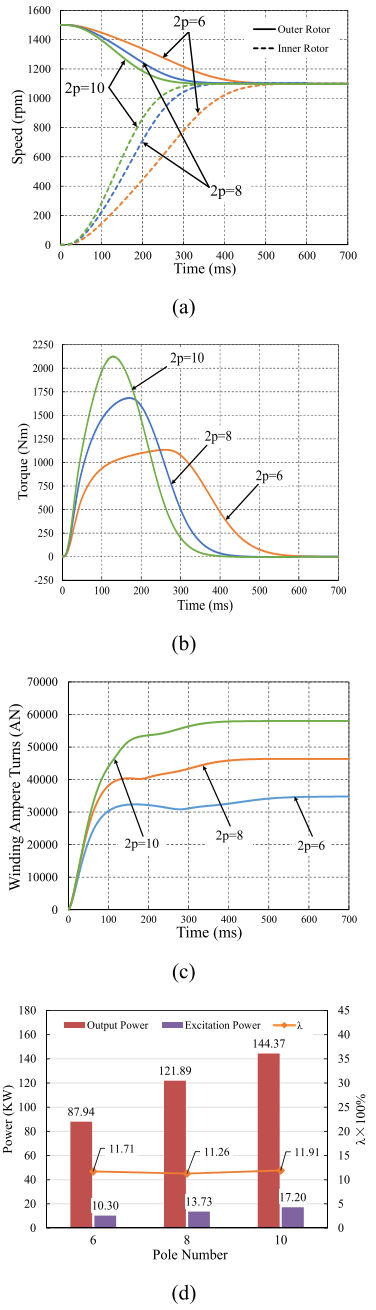

FIGURE 7. Performance comparison of DRIM with different pole number. (a) Rotor speed. (b) Torque. (c) Winding ampere turns. (d) Power comparison.

B. COIL TURNS

Transient performances of different DRIMs when excitation coil turns is 40, 80, and 120 are obtained by 2D FEM in this subsection. Total winding resistance is assumed to be directly proportional to coil turns number here. Then total winding resistance is 1.31 Ω for 40 turns, 2.62 Ω for 80 turns, and 3.93 Ω for 120 turns, respectively

The DC excitation voltage fed on the excitation winding of different models is adjusted according to the difference of winding resistance, so that the maximum total winding ampere turns of different models remains identical. Here maximum excitation current I is 145.0A for 40 turns, 72.5A for 80 turns, and 48.3A for 120 turns. And excitation voltage is kept to 190V for different models. The other parameters is consistent with Table 1. The simulation results are shown in Fig. 8.

As shown in Fig. 8(c), even though the maximum winding ampere turns is identical, the establishment of winding ampere turns speeds down with the increase of coil turns. As a result, the torque establishment is speeding down with the increase of coil turns as shown in Fig. 8(b). And the maximum torque also slightly decreases with the increase of

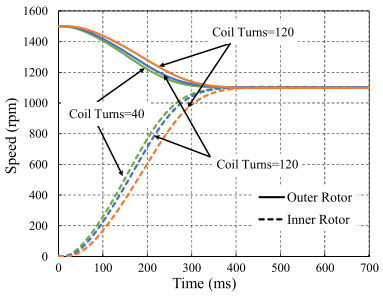

(a)

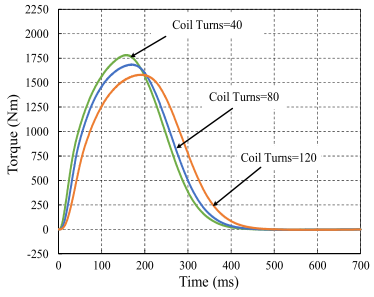

(b)

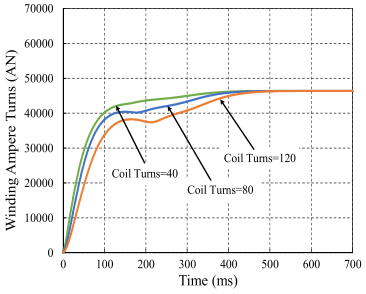

(c)

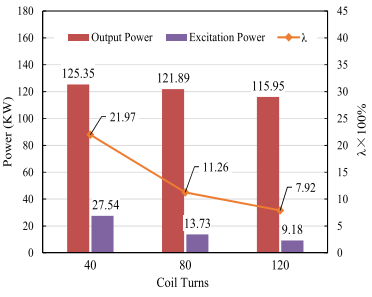

(d)

FIGURE 8. Performance comparison of DRIM with different number of coil turns. (a) Rotor speed. (b) Torque. (c) Winding ampere turns. (d) Power comparison.

coil turns, i.e. 1778 Nm for 40 turns, 1685 Nm for 80 turns, and 1580 Nm for 120 turns. Hysteresis of maximum torque also appears along with the increase of coil turns. However, it can be observed from Fig. 8(a) that the time required by the inner rotor to reach the final speed Ω_f is almost identical.

Fig. 8(d) shows a comparison between maximum driving power and required excitation power of DRIM with different coil turns. It can be seen that both the two maximum power

(a) (b)

FIGURE 9. Manufactured rotors of DRIM prototype. (a) Outer rotor with excitation winding. (b) Inner rotor.

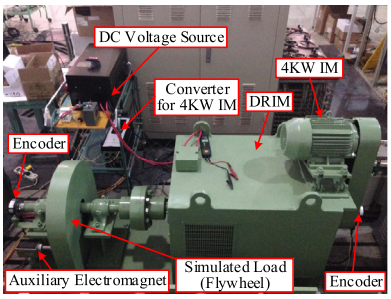

FIGURE 10. Established experiment platform of the novel PPDS based on the DRIM.

increase along with decrease of coil turns. But the augment of maximum excitation power is more noticeable so the factor λ also augments. But a lower coil turns number also leads to a higher excitation current. Considering the necessary transient driving ability and the current limitation of the excitation source, an 80 coil turns design scheme is selected in the following prototype design.

VI. EXPERIMENT VALIDATION

Main parameters of the prototype are consistent with Table 1. Fig. 9(a) and Fig. 9(b) show the manufactured outer rotor with the excitation winding and the inner rotor, respectively. Fig.10 shows the experiment platform. A 4 KW induction motor is connected to input shaft of DRIM by a belt pulley. The output shaft of DRIM is connected to a flywheel load by a coupling joint. And an electromagnet is installed near the flywheel to serve as the auxiliary locking device.

Main experiment steps are as follows. Firstly, outer rotor is driven to predetermined speed of 1500 rpm by the induction motor while the inner rotor is kept standstill by the auxiliary locking device. After that, the source of the induction motor is turned off and the locking device is unlocked. Then a 190 V DC voltage is fed to the excitation winding of DRIM, and the voltage source is cut off after 500 ms. Experiment and its corresponding simulation results are shown in Fig. 11.

As shown in Fig. 11(a), it takes inner rotor about 410 ms to reach the target speed of 1100 rpm. And according to simulation results shown in Fig. 11(b) the inner rotor reach final speed of 1100 rpm in 422 ms. A well agreement between experiment and simulation results is achieved.

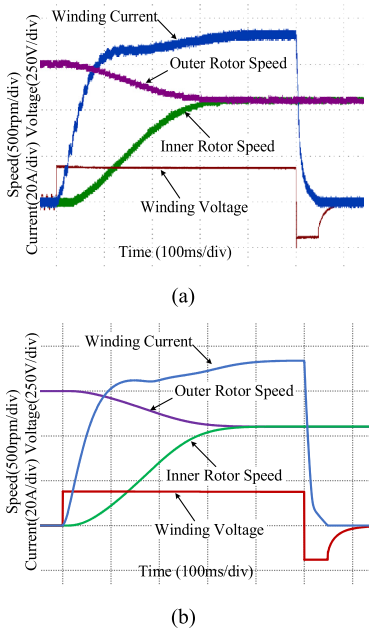

FIGURE 11. Performance of the DRIM when $U = 190$ V, $\Omega_0 = 1500$ rpm. (a) Experiment results. (b) Simulation results.

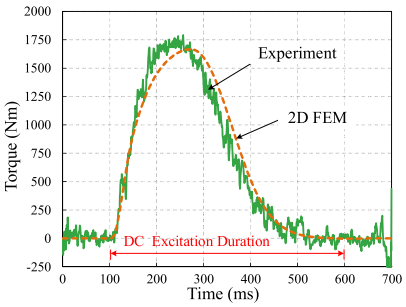

FIGURE 12. DRIM transient torque curves obtained by experiment and simulation.

TABLE 2. Experiment and simulation results of the prototype.

Item	Experiment	2D FEM
Maximum driving power P_{M2}/KW	120.75	121.89
Maximum excitation power P_{1e}/KW	14.12	13.73
Power ratio λ	11.69%	11.26%

A one-order tracking differentiator is employed to obtain the transient angular accelerator of inner rotor based on its experiment speed data. The transient torque of DRIM is then obtained by (8) and depicted in Fig. 12. The driving power is calculated by (10). The maximum driving power and required excitation power obtained by the experiment and 2D FEM simulation are listed in Table 2.

From Fig. 12 and Table 2, it is known that the transient torque, the maximum driving power, the excitation power, and the power ratio calculated by the simulation agree well with experiment results. The difference is mainly attributed to the rotational inertia measurement error and the neglecting of axial friction in the established simulation model.

VII. CONCLUSION

The DRIM proposed in this paper can directly utilize the rotational kinetic energy stored in the outer rotor to accelerate the inertia load through the electromagnetic torque. The large power converter and the large power driving motor are no longer needed though the substitution of the MGFW with the DRIM in the PPDS.

Since only a DC voltage is required by the DRIM in the driving stage, the operation control of the DRIM is simple.

The maximum excitation power required by the DRIM is very small compared with its maximum mechanical driving power. So the electrical ratings of the converter in the PPDS based on the DRIM can be reduced. This is good for improving the system compactness of the PPDS.

The driving performance of a DRIM can be improved by increasing the pole number and decreasing coil turns within a certain range. And the power ratio λ is also influenced by these two structure parameters. So a reasonable compromise is needed in the final determination of the pole number and the coil turns. This provides the theory guidance for the further research on the design optimization of the DRIM.

Even though the eddy current loss in the inner rotor of the DRIM leads to a relatively low efficiency, considering the intermittent operation mode of the DRIM and the system simplification achieved by it, a sacrifice of efficiency is still acceptable in order to improve the compactness of the whole system, especially for the PPDS deployed in mobile platforms with limited space and weight-carrying capacity.

REFERENCES

[1] D. W. Swett and J. G. Blanche, "Flywheel charging module for energy storage used in electromagnetic aircraft launch system," *IEEE Trans. Magn.*, vol. 41, no. 1, pp. 525–528, Jan. 2005. doi: 10.1109/TMAG.2004.838745.

[2] G. Becherini, S. D. Fraia, and B. Tellini, "Modeling and analysis of a multistage linear induction motor fed by a permanent magnet flywheel motor-generator," in *Proc. Int. Conf. Elect. Mach. Syst. (ICEMS)*, Rome, Italy, Sep. 2010, pp. 1–6. doi: 10.1109/ICELMACH.2010.5608102.

[3] C. Ye, K. Yu, W. Xu, and H. Zhang, "Optimal design and experimental research of a capacitor-charging pulsed alternator," *IEEE Trans. Energy Convers.*, vol. 30, no. 3, pp. 948–956, Sep. 2015. doi: 10.1109/TEC.2015.2395446.

[4] A. Balikci, Z. Zabar, D. Czarkowski, E. Levi, and L. Birenbaum, "Flywheel motor/generator set as an energy source for coil launchers," *IEEE Trans. Magn.*, vol. 37, no. 1, pp. 280–283, Jan. 2001. doi: 10.1109/20.911837.

[5] M. Giesselmann, B. McHale, and M. Crawford, "Fast, transient energy extraction from high-frequency AC alternators for use in electromagnetic launch applications," *IEEE Trans. Magn.*, vol. 41, no. 1, pp. 289–293, Jan. 2005. doi: 10.1109/TMAG.2004.839279.

[6] K. Liu, M. Yin, W. Hua, Z. Ma, M. Lin, and Y. Kong, "Design and analysis of Halbach ironless flywheel BLDC motor/generators," *IEEE Trans. Magn.*, vol. 54, no. 11, Nov. 2018, Art. no. 8109305. doi: 10.1109/TMAG.2018.2833958.

[7] K. Liu, M. Yin, W. Hua, Z. Ma, M. Lin, and Y. Kong, "Design and optimization of an external rotor ironless BLDCM used in a flywheel energy storage system," *IEEE Trans. Magn.*, vol. 54, no. 11, Nov. 2018, Art. no. 8109105. doi: 10.1109/TMAG.2018.2837098.

[8] X. Zhang and J. Yang, "A robust flywheel energy storage system discharge strategy for wide speed range operation," *IEEE Trans. Ind. Electron.*, vol. 64, no. 10, pp. 7862–7873, Oct. 2017. doi: 10.1109/TIE.2017.2694348.

[9] B. Anvari, X. Li, H. A. Toliyat, and A. Palazzolo, "A coreless permanent-magnet machine for a magnetically levitated shaft-less flywheel," *IEEE Trans. Ind. Appl.*, vol. 54, no. 5, pp. 4288–4296, Sep./Oct. 2018. doi: 10.1109/TIA.2018.2839747.
[10] X. Li, B. Anvari, A. Palazzolo, Z. Wang, and H. Toliyat, "A utility-scale flywheel energy storage system with a shaftless, hubless, high-strength steel rotor," *IEEE Trans. Ind. Electron.*, vol. 65, no. 8, pp. 6667–6675, Aug. 2018. doi: 10.1109/TIE.2017.2772205.
[11] K.-H. Kim, H.-I. Park, S.-M. Jang, and J.-Y. Choi, "Comparison of characteristics of double-sided permanent-magnet synchronous motor/generator according to magnetization patterns for flywheel energy storage system using an analytical method," *IEEE Trans. Magn.*, vol. 51, no. 3, Mar. 2015, Art. no. 8201404. doi: 10.1109/TMAG.2014.2358791.
[12] B. Fan, C. Wang, Q. Yang, W. Liu, and G. Wang, "Performance guaranteed control of flywheel energy storage system for pulsed power load accommodation," *IEEE Trans. Power Syst.*, vol. 33, no. 4, pp. 3994–4004, Jul. 2018. doi: 10.1109/TPWRS.2017.2774273.
[13] H. A. Moghaddam, A. Vahedi, and S. H. Ebrahimi, "Design optimization of transversely laminated synchronous reluctance machine for flywheel energy storage system using response surface methodology," *IEEE Trans. Ind. Electron.*, vol. 64, no. 12, pp. 9748–9757, Dec. 2017. doi: 10.1109/TIE.2017.2716877.
[14] J. Park, C. Kalev, and H. F. Hofmann, "Control of high-speed solid-rotor synchronous reluctance motor/generator for flywheel-based uninterruptible power supplies," *IEEE Trans. Ind. Electron.*, vol. 55, no. 8, pp. 3038–3046, Aug. 2008. doi: 10.1109/TIE.2008.918583.
[15] C. Ye, J. Yang, W. Xu, F. Xiong, and X. Liang, "A novel multi-unit out-rotor homopolar inductor machine for flywheel energy storage system," *IEEE Trans. Magn.*, vol. 54, no. 11, Nov. 2018, Art. no. 8204505. doi: 10.1109/TMAG.2018.2834956.
[16] Y. Liu, L. Shi, L. Zhao, and Y. Li, "The controls of motors in flywheel energy storage system," in *Proc. 9th IEEE Conf. Ind. Electron. Appl. (ICIEA)*, Hangzhou, China, Jun. 2014, pp. 179–182. doi: 10.1109/ICIEA.2014.6931154.
[17] H. Zhu, L. Zhao, Y. Liu, and L. Shi, "Unity power factor control strategy of electrically excited synchronous motor fed by high power back-to-back converter," in *Proc. 18th Int. Conf. Elect. Mach. Syst. (ICEMS)*, Pattaya, Thailand, Oct. 2015, pp. 223–226. doi: 10.1109/ICEMS.2015.7385031.
[18] Y. Liu, L. Shi, L. Zhao, and Y. Li, "The FOC and DTC scheme in a high power electrically excited synchronous motor based flywheel energy storage system," in *Proc. Int. Power Electron. Appl. Conf. Expo. (PEAC)*, Shanghai, China, Nov. 2014, pp. 1333–1338. doi: 10.1109/PEAC.2014.7038056.
[19] W. Keyin, L. Dezhi, M. Jin, O. Yangbin, Z. Xiaofei, and C. Junquan, "Design and simulation of a 12-phase flywheel energy storage generator system with linearly dynamic load," *IEEE Trans. Appl. Supercond.*, vol. 20, no. 3, pp. 1050–1054, Jun. 2010. doi: 10.1109/TASC.2010.2040599.
[20] C. Wang, H. Li, M. Bu, W. Li, Y. Wang, and W. Xuan, "Implementation of an excitation controller for an impulse motor-generator," *IEEE Trans. Plasma Sci.*, vol. 46, no. 5, pp. 1694–1698, May 2018. doi: 10.1109/TPS.2018.2794964.
[21] T. Lubin and A. Rezzoug, "Steady-state and transient performance of axial-field eddy-current coupling," *IEEE Trans. Ind. Electron.*, vol. 62, no. 4, pp. 2287–2296, Apr. 2015. doi: 10.1109/TIE.2014.2351785.
[22] J. Wang, H. Lin, and S. Fang, "Analytical prediction of torque characteristics of eddy current couplings having a quasi-Halbach magnet structure," *IEEE Trans. Magn.*, vol. 52, no. 6, Jun. 2016, Art. no. 8001209. doi: 10.1109/TMAG.2016.2529587.
[23] T. Lubin and A. Rezzoug, "Improved 3-D analytical model for axial-flux eddy-current couplings with curvature effects," *IEEE Trans. Magn.*, vol. 53, no. 9, Sep. 2017, Art. no. 8002409. doi: 10.1109/TMAG.2017.2714628.
[24] R. L. Russell and K. H. Norsworthy, "Eddy currents and wall losses in screened-rotor induction motors," *Proc. IEE A, Power Eng.*, vol. 105, no. 20, pp. 163–175, Apr. 1958. doi: 10.1049/pi-a.1958.0036.

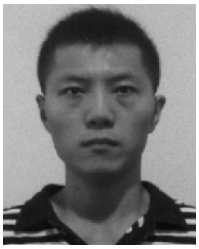

PEILONG WANG received the B.Eng. and M.Sc. degrees from Henan Polytechnic University, Jiaozuo, China, in 2011 and 2014, respectively. Since 2015, he is currently pursuing the Ph.D. degree in electrical engineering with the Institute of Electrical Engineering, Chinese Academy of Sciences, Beijing, China.

His research interest includes design and control of novel electrical machines.

LIMING SHI (M'12) received the M.S. degree in electrical engineering from the Graduate School of Chinese Academy of Sciences, Beijing, China, in 1990, and the Ph.D. degree in electrical engineering from Kyushu University, Fukuoka, Japan, in 1998.

From 1998 to 2000, he was a Postdoctoral Research Fellow at the Japan Society for the Promotion of Sciences, Japan. From 2000 to 2002, he was the Chief Researcher with Yaskawa Electric Company, Ltd., Kitakyushu, Japan. He joined the Institute of Electrical Engineering, Chinese Academy of Sciences, Beijing, China, in 2002, where he is currently a Professor. His current research interests include analysis and control of electrical machines and wireless power transfer technology.